REPORT DOCUMENTATION PAGE

Form Approved
OMB No. 0704-0188

1. REPORT DATE *(DD-MM-YYYY)*	2. REPORT TYPE	3. DATES COVERED *(From - To)*
13-01-2009	Final Technical Report	Aug 15, 2007 - Aug 14, 2008

4. TITLE AND SUBTITLE
Microelectronic Precision Optical Element Fabrication

5a. CONTRACT NUMBER

5b. GRANT NUMBER
HR0011-07-1-0039

5c. PROGRAM ELEMENT NUMBER

6. AUTHOR(S)
Goossen, Keith W.

5d. PROJECT NUMBER

5e. TASK NUMBER

5f. WORK UNIT NUMBER

7. PERFORMING ORGANIZATION NAME(S) AND ADDRESS(ES)
University of Delaware - Electrical & Computer Engineering Dept.
140 Evans Hall
Newark, DE 19716

8. PERFORMING ORGANIZATION REPORT NUMBER
ELEG332241-1-13-09

9. SPONSORING/MONITORING AGENCY NAME(S) AND ADDRESS(ES)
Defense Advanced Research Project Agency (DARPA)
Contracts Management Office (CMO)
3700 North Fairfax Drive
Arlington, VA 22203-1714

10. SPONSOR/MONITOR'S ACRONYM(S)

11. SPONSOR/MONITOR'S REPORT NUMBER(S)

12. DISTRIBUTION/AVAILABILITY STATEMENT
Approved for public release; distribution is unlimited

13. SUPPLEMENTARY NOTES

14. ABSTRACT
The DARPA program involved investigating the assembly of 3-dimensional optoelectronic/microelectronic components with optical precision. A three-active-facet retromodulator with multiple quantum well modulators on the three faces of a corner cube was constructed. The corner cube was made using FR4 printed circuit boards (PCB's) utilizing standard microelectronic machining equipment. An active retromodulator, utilizing large-area multiple quantum well modulators on 3 faces, was demonstrated, and a high modulation contrast ratio of 8.23dB was shown to be achievable. The large-area devices were fabricated using substrates made by metalorganic chemical vapor deposition. The proposed target angular error in the module face angles was +/- 0.5 degrees. However, errors of +/- 1 degree were achieved in the corner cube modules. These angular errors can be corrected by using readily available off-the-shelf optical components to achieve true retroreflection, with additional bulk to the system. Alternatively, the PCB's can be mounted directly upon a precision corner cube with additional cost to the system. The large-area multiple quantum well devices fabricated from substrates grown using MOCVD have a lower defect density than those grown using MBE.

15. SUBJECT TERMS
Geometrical optics, Optoelectronics, Microelectronic packaging, Free-space optical communication

16. SECURITY CLASSIFICATION OF:			17. LIMITATION OF ABSTRACT	18. NUMBER OF PAGES	19a. NAME OF RESPONSIBLE PERSON
a. REPORT	b. ABSTRACT	c. THIS PAGE			Keith W. Goossen
U	U	U	UU	21	19b. TELEPHONE NUMBER *(Include area code)* (302) 831-0590

Microelectronic Precision Optical Element Fabrication
Final Technology Report

Technical Area: **Microsystems addressing challenges in complex systems architectures**

Prepared for: **Dr. Joseph Mangano**
Program Manager, DARPA-MTO
3701 N. Fairfax Drive, Arlington, VA 22203-1714

Lead Organization: **University of Delaware (Other Educational)**
Electrical and Computer Engineering Department
140 Evans Hall, Newark, DE 19716
Taxpayer ID: 51-6000297

Technical POC: **Keith W. Goossen**
Principal Investigator
Electrical and Computer Engineering Department
140 Evans Hall, Newark, DE 19716
Phone: (302) 831-0590
Fax: (302) 831-4316
Email: goossen@ece.udel.edu

Admin. POC: **Susan D. Tompkins**
Contract & Grant Administrator
Research Office
210 Hullihen Hall, Newark, DE 19716
Phone: (302) 831-8002
Fax: (302) 831-2828
Email: sdt@udel.edu

DARPA Award #HR0011-07-1-0039:
Microelectronic Precision Optical Element Fabrication

Abstract: *The DARPA program involved investigating the assembly of three dimensional optoelectronic/microelectronic components with optical precision. As a test vehicle we attempted to construct a three-active-facet retromodulator with multiple quantum well modulators on the three faces of a corner cube. The corner cube was made using FR4 printed circuit boards (PCB's) utilizing standard microelectronic machining equipment. We demonstrate an active retromodulator which utilizes large-area multiple quantum well modulators on the three faces and show that a high modulation contrast ratio of 8.23dB can be achieved. The large-area devices were fabricated using substrates made by metalorganic chemical vapor deposition. The proposed target angular error in the module face angles was ±0.5°. However, we achieved errors of ±1° in the corner cube modules that were constructed. We show that these angular errors can be corrected for by using readily available off-the-shelf optical components to achieve true retroreflection, with additional bulk to the system. Alternatively, the PCB's can be mounted directly upon a precision corner cube, with additional cost to the system. Additionally, we show that the large-area multiple quantum well devices fabricated from substrates grown using MOCVD have a lower defect density than those grown using MBE.*

Keywords: *Geometrical optics, Optoelectronics, Microelectronic packaging, Free-space optical communication*

Contents

1. Introduction

Modulated retroreflectors (MRR) have several military and commercial applications which include low-power communication with ultralight air vehicles [1], space-to-ground optical communication [2], remote telemetry [3], distance measurement [4], dynamic optical tags for equipment and personnel [5] and potentially, on–road vehicle–to–vehicle communication for accident prevention [6]. For communication applications, the MRR's can have advantages over radio links in terms of power dissipation and selectivity. The applications listed above and others require the construction of three dimensional optics and electronics with optical precision [7].

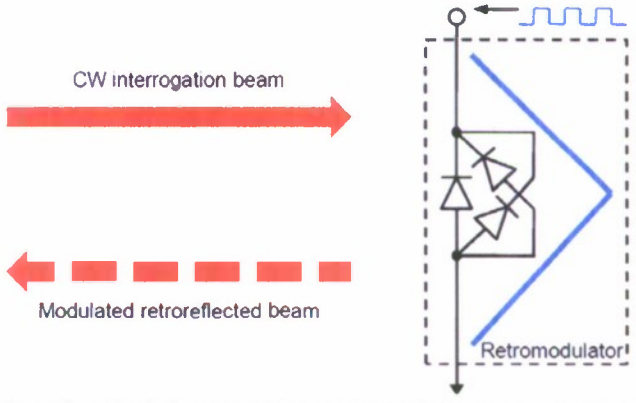

Fig. 1. Schematic showing the MQW diode configuration in the retromodulator. The three diodes are connected in parallel.

In the past, there have been several approaches to build retromodulators. Microelectromechanical (MEMS) elements such as deformable mirrors [3], variable etalons [8], [9], or deformable gratings [10] have been used as the modulating element where the MEMS component is basically one of the faces of the corner cube. Another general approach is to use some sort of shutter as the aperture of a precision milled corner cube such as a ferro liquid crystal [11]. Semiconductor modulators can be also be used as the retromodulator shutter [1] or as one of the faces of the corner cube. The semiconductor modulators are typically in the form of p-i-n diodes where the intrinsic region consists of a multiple quantum wells (MQW). MQW devices exploit the quantum confined Stark effect (QCSE) and are efficient electroabsorption modulators [12]. The semiconductor devices can offer higher bandwidth and higher

angular tolerance than MEMS devices. In [1], a transmission–mode MQW modulator was placed at the aperture of a precision milled retroreflector. Such a setup may have reliability issues since the brittle MQW substrate is free standing and may be highly prone to damage, especially in some military applications. Additionally, the use of the precision milled corner cube host block may not be cost effective.

In this work, we consider using three large–area MQW devices on the three faces of the corner cube. We attempt to use well–developed microelectronic packaging technology to assemble the module. The MQW devices can be mounted on standard FR4 printed circuit boards (PCB) and assembled together so that there are modulators on all three faces of the retroreflector. The advantage of using PCBs is that it is easier to provide electrical connections to bias the devices since tracing metal lines on FR4 boards is a well developed process. Additionally, the boards provide mechanical strength to the brittle device substrates. While it may be challenging to assemble the PCBs together so that they are exactly orthogonal to each other we show that readily available, off-the-shelf optical components can be used to correct for the angular errors in the retromodulator. This approach enables the use of modulators on all three faces as shown in the schematic in Figure 2. So a higher contrast ratio (CR) can be achieved. The design and characterization of the large–area MQW devices is described in the next section. The construction and the experimental demonstration of the PCB-based retromodulator is discussed in section III which is followed by a section that discusses the corrective optics needed for the PCB–based retromodulator. Finally, in section V, we discuss the feasibility of using three modulating devices on the three faces of a precision milled corner cube.

2. Large-Area Multiple Quantum Well Devices

The quantum well devices used in this work are designed to operate at around 1.55μm. The yield of GaAs–based modulators operating at 0.85μm can be high [13]. But since the application targeted here involves free space optical propagation the longer wavelength InP–based devices are chosen for eye

safety. The wafer with layer structure shown in Figure 2 was grown by metalorganic chemical vapor deposition (MOCVD) by IQE Inc. The intrinsic region of the p–i–n diode consists of 150 85Å InGaAs wells separated by 35 Å InAlAs barriers lattice matched to InP. The p–i–n layers were grown on a n–type InP substrate. Ti–Au (150Å/2000Å) contacts were deposited by evaporation and lift–off to form the top contacts of the devices. The device mesas, with dimensions 3.3mm x 3.3mm, were created by etching 1μm into the substrate. A silicon monoxide antireflective coating was deposited on the optical window of the devices using lift-off. A 2000Å silver film was evaporated on the backside of the wafer to enable the use of the MQW devices in reflection mode and hence no separate bottom contacts were necessary. Finally, the individual large–area devices were diced apart.

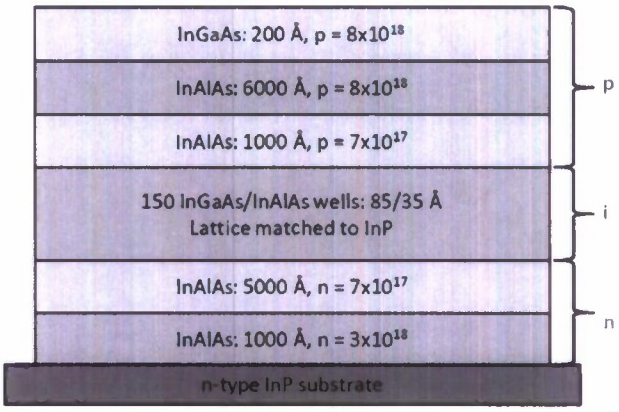

Fig. 2. Layer structure of the MQW modulator.

a. Device yield

Yield is an important parameter to be considered during device fabrication. A total of 61 large–area quantum well devices were fabricated. The leakage currents for all the devices were measured and the distribution is shown in Figure 3. About 62% of the devices show excellent diode characteristics and have leakage currents below 300μA at a reverse bias of 15V. At this bias, we observed catastrophic leakage currents of >5mA in 26% of the devices. Hence, the areal defect density was calculated to be 2.4 defects/cm^2. This is lower than the defect density achieved with similar large–area devices fabricated using molecular beam epitaxy [14]. As shown in Figure 3, some of the devices had leakage currents

between 100μA and 1mA. The usability of these devices will depend on the power specifications and heat sinking capabilities of the intended application.

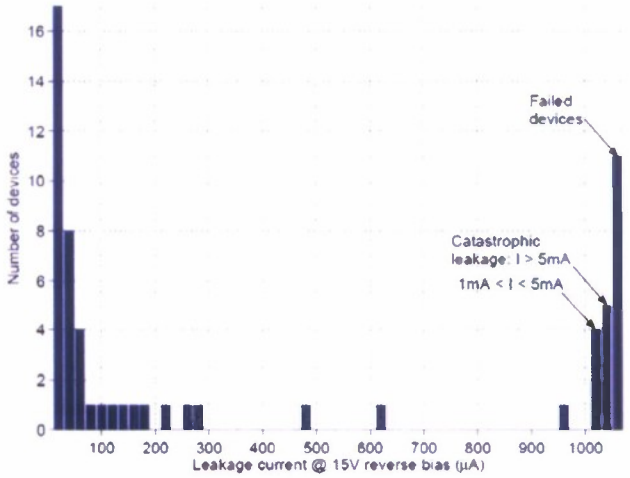

Fig. 3. Leakage current distribution of fabricated MQW diodes with a 15V reverse bias.

b. MQW diode electrical and optical characteristics

In applications where a set of MRR's are used along with a laser to enable a bidirectional free–space optical communication link, a low dark current is desired in order to have high receiver sensitivity. The reverse bias I–V characteristic of one of the fabricated MQW diodes is shown in Figure 4. At a reverse bias of 20V, the dark current, I_{Dark}, is less than 50μA which corresponds to a static power dissipation of 3mW per module. Also shown in Figure 4 is the reflection spectrum of the device at varying reverse bias voltages. The measurement was done with the device tilted at about 35° to the optical axis since in retromodulator module the light will always

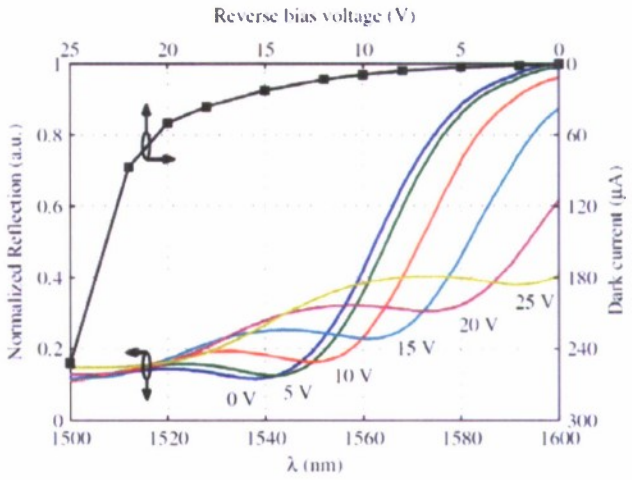

Fig. 4. Modulator reflection spectra for a 0-25V reverse bias and the device tilted at ~35° to the optical axis. Also shown is the diode reverse bias I-V curve.

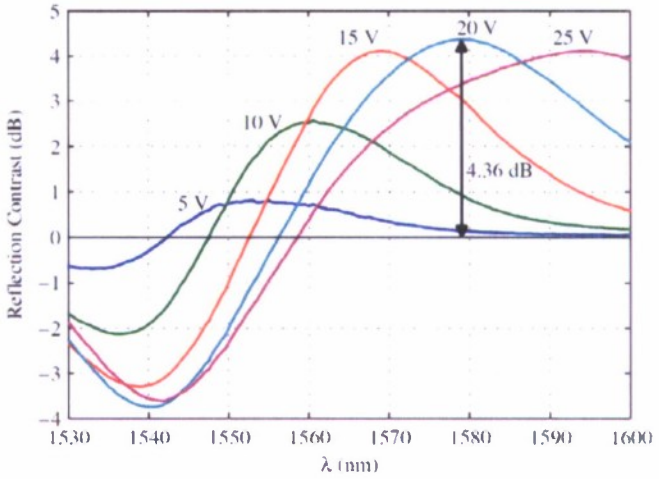

Fig. 5. Modulator reflection contrast for a 0-25V reverse bias. A maximum of 4.36dB is observed at λ = 1579nm for a reverse bias of 20V.

be incident on the device at an oblique angle. The measured reflection contrasts for the device is shown in Figure 5. A maximum reflection contrast of 4.36dB is observed with a reverse bias of 20V at λ = 1579nm. A low insertion loss of 0.614dB is observed. Similarly, at lower reverse bias voltages of 10V and 15V, reflection contrasts of 2.56db and 4.12dB are observed at wavelengths 1560.5nm and 1569nm respectively. With the triple–modulator retroreflector configuration, the system can potentially deliver a total of 7.68dB, 12.36dB and 13.08dB contrast ratios at 10, 15 and 20V respectively. Hence, depending

on the power–modulation trade off specifications for a given application, a higher or lower operating voltage can be used.

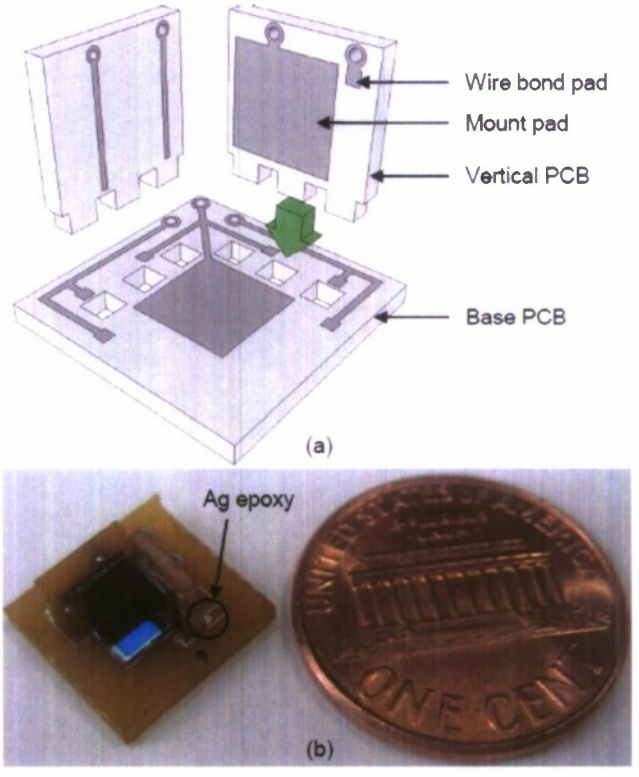

Fig. 6. (a) Pronged PCB schematic. The vertical board on the left is rotated by 180° to illustrate the back side metal traces. (b) The PCB-based retromodulator module with the MQW devices die bonded on the boards.

3. Printed Circuit Board-Based MRR

Standard FR4 printed circuit boards can be used to build the MRR module. The schematic of the module is shown in Figure 6a. Fingers were milled on the vertical PCBs using a standard table top mill. Machining was does so that the vertical PCB fit tightly into the base PCB. The individual large–area MQW modulators were bonded on the metal mounting pad using a silver epoxy adhesive from Epoxy Technology. After curing the epoxy at about 80°C for 15 minutes, the top metal contact of the MQW modulators were wire bonded to the PCB bond pad. The module was then assembled together. The silver epoxy was again used to connect the metal traces on the back side vertical PCB to the pads on the base PCB. The final assembled module is shown in Figure 6b. Similar PCBs modules were assembled with

plane mirrors on the three faces to measure the angles between the faces. The angle between the two vertical faces is 90°. The angle between the two vertical PCBs and the base lies between ±0.5°. This deviation from 90° has a detrimental effect on the performance of the retroreflector. Using more precise milling equipment for machining the PCBs may result is smaller angular errors. However, simple optical components can be used to correct for these errors. The corrective optics is discussed in section IV.

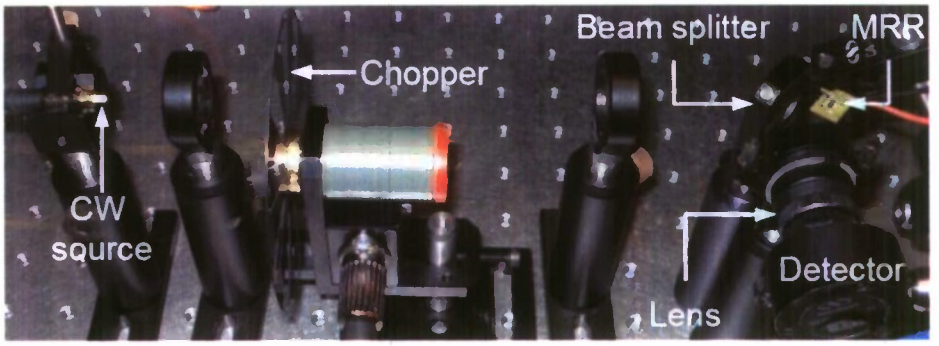

Fig. 7. MRR experimental setup.

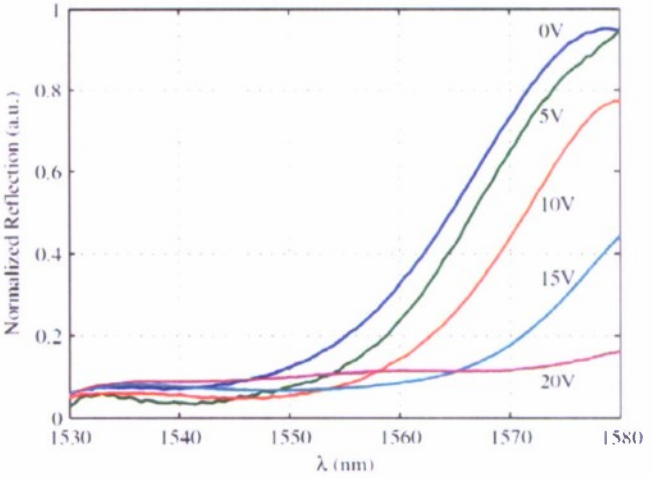

Fig. 8. MRR retroreflection spectra for reverse bias 0-20V.

a. MRR experimental results

The assembled MRR was tested using the setup shown in Figure 7. A CW tunable laser was used to interrogate the MRR with the source wavelength varying from 1530nm to 1580nm. A beam splitter was used to redirect the retroreflected beam to a photodetector. The retroreflected photocurrent was measured using a lock–in amplifier with the chopper being the reference. The measured reflection spectra for bias

voltages of 0–20V are shown in Figure 8. The reflection contrast is shown in Figure 9. With a reverse bias of 20V, a CR of about 7:1 is observed at a wavelength $\lambda = 1574$nm. This is a higher CR than [1].

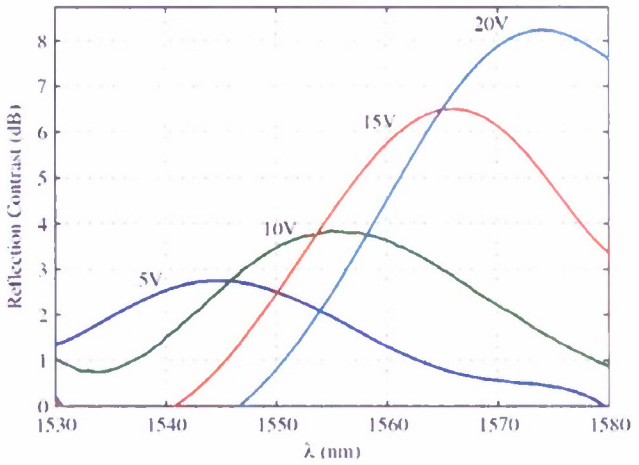

Fig. 9. MRR reflection contrast. A maximum contrast of 8.23dB is observed at $\lambda = 1574$nm with a bias of 20V.

4. Optical Correction System (PCB-MRR)

We observed that we could limit the face angular error to $\pm 1°$ in the constructed FR4 corner–cubes. This small error, however, has a detrimental effect to the proper operation of the retroreflector. To test the corner–cubes, plane silver mirrors (8.2mm x 8.2mm) were mounted on the three faces using the low viscosity epoxy TRA-BOND 931-1 from TRA-CON, Inc. This epoxy was chosen as the adhesive so that it flows evenly between the mount pad and the mirror during the curing process to minimize its contribution to the angular error. The epoxy was allowed to cure at room temperature for 24 hours after which the three mirrored-boards were assembled together to form the retroreflector. One such assembled module after all the mirrors were mounted on the three boards is shown in Figure 10. Here, α and β were measured to be $89.5°$ while γ was $90°$. While it may be challenging to make all three faces exactly orthogonal to

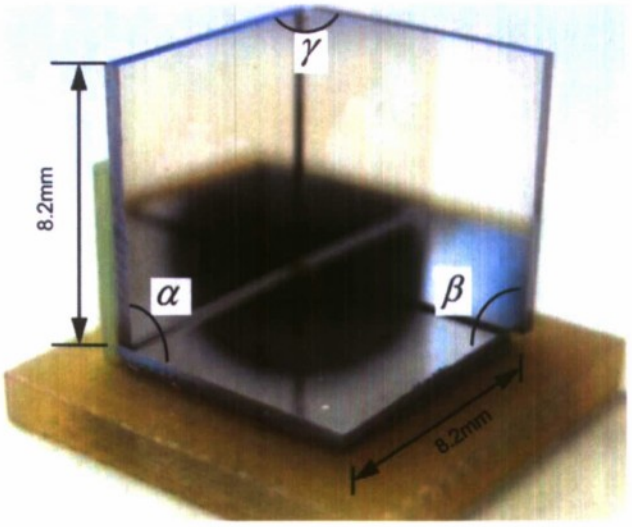

Fig. 10. Assembled corner--cube module with silver mirrors mounted on all three faces. The angles between the faces, α, β, and γ, are indicated.

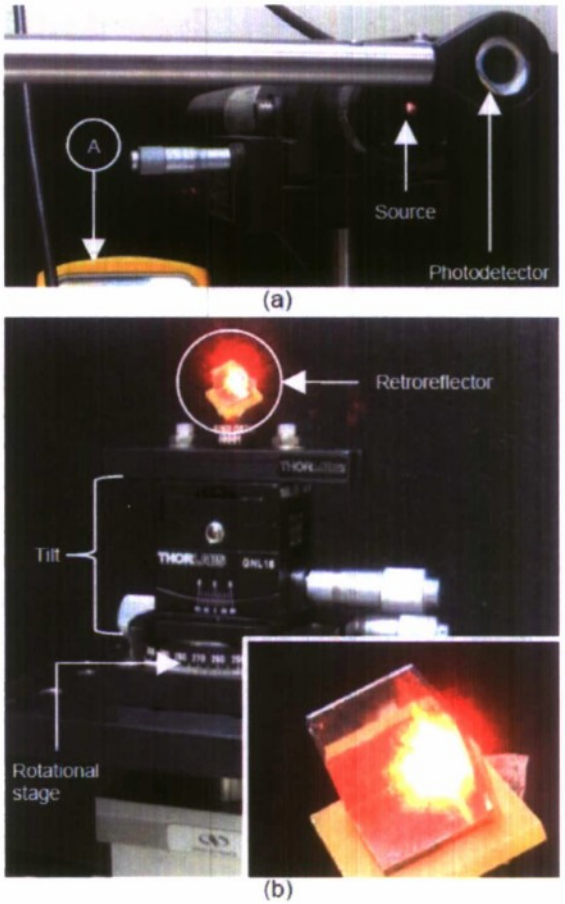

Fig. 11. Setup to test the uncorrected imperfect retroreflector. (a) The source-detector setup. (b) The retroreflector setup. The inset at the bottom right shows the illuminated module.

each other, careful machining may result in a lower angular error in α and β. This 'imperfect' retroreflector (IRR) was illuminated using a HeNe laser from a distance of about 2.5m using the set up shown in Figure 11. As shown in Figure 12, the angular imperfections in the retroreflector results in multiple spots on the observation plane; all of which are diverging away from the optical axis. There are multiple retroreflected spots on the observation plane in Figure 3 because the interrogation beam illuminates all three faces of the corner cube simultaneously resulting in multiple retroreflection pathways. This IRR was modeled in LightTools® by Optical Research Associates (ORA®) which is a three dimensional ray tracing software. The source and detector was set at a distance of 2.5m from the IRR. At a distance of only 2.5m, the "retroreflected" spots are approximately 32mm away from the optical axis. The horizontal and vertical rotation of the IRR results in the spot moving around this center location. No optical power is retroreflected back to a detector that is located on the optical axis. Any correction system that is introduced will require the multiple diverging beams to be redirected back to the optical axis as shown schematically in Figure 13. It should also be tolerant to the rotation of the IRR that it is designed for so as to allow for imperfect alignment in the applications such as military identification systems on the battlefield. For this work, the theoretical modeling is done using an annular detector with the laser source in the middle. Another possible approach is to use a single round or square-shaped detector located next to the source. However, in that case the orientation of the IRR becomes critical. While a correction system could be designed and optimized with the adjacent detector, if the IRR were rotated by 180° in the plane orthogonal to the optical axis, the performance of the IRR is significantly diminished.

a. Optical correction system design

The annular detector used in the theoretical modeling of the correction system has an inner and outer radius of 1mm and 10mm respectively. The correction system must be designed for an IRR that is offset from the optical axis so that the interrogating beam hits one of the faces and

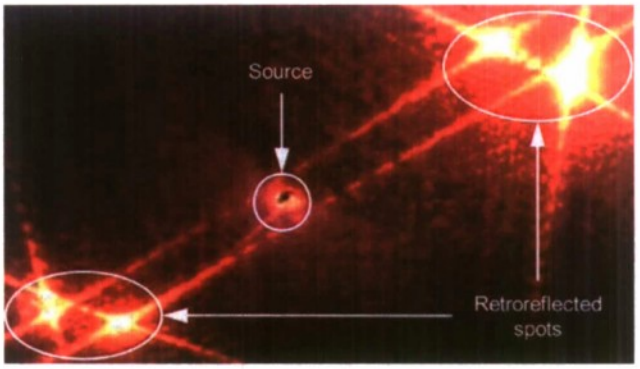

Fg. 12. Result of illuminating the IRR from a distance of 2.5m. The shown observation plane is located just in front of the source. No light is retroreflected to the center of the observation plane.

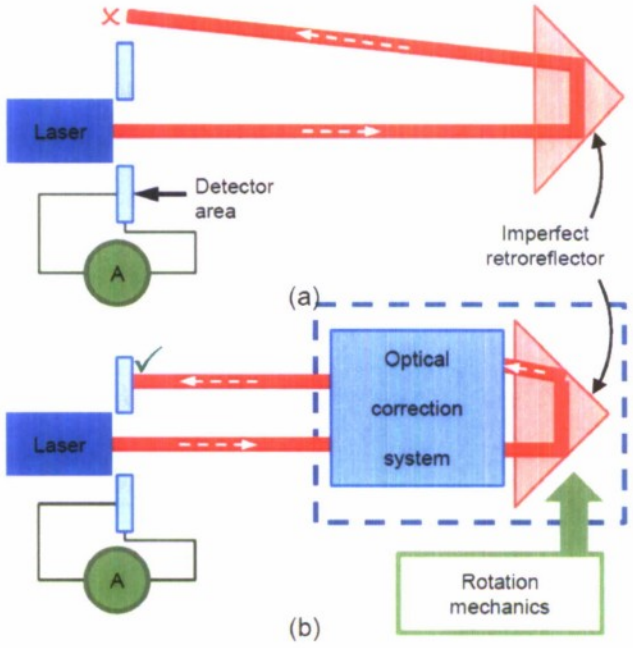

Fig. 13. Schematic showing the retroreflection system (a) without and (b) with the optical correction system.

not the vertex of the module. During the PCB assembly, gaps may be introduced between the mirrors due to imperfect alignment resulting in the leakage of the interrogating laser beam. More importantly, in practical realizations of this PCB-based retroreflector, the three faces may have modulators to modulate the interrogating beam. The active area of such devices does not typically extend to the edge of the

device. Hence, any light incident along the edges of the devices is effectively "wasted" and the CR is significantly diminished.

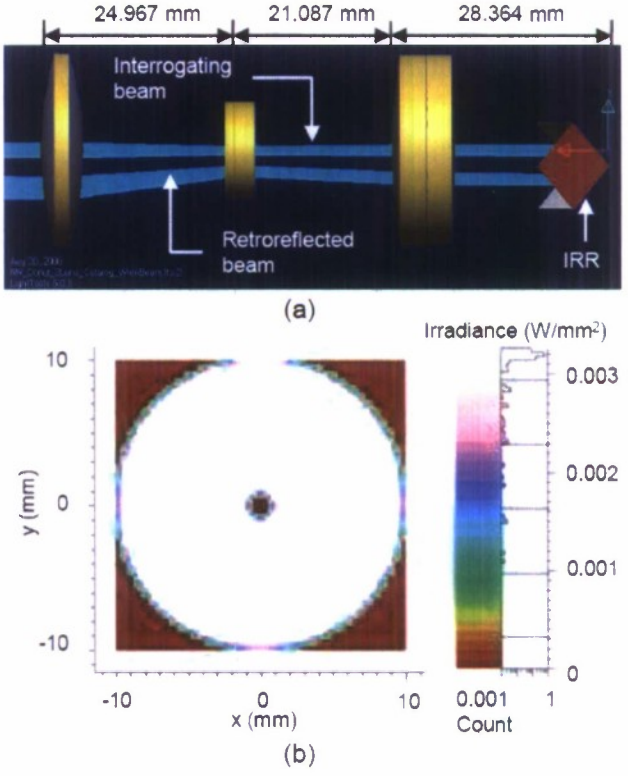

Fig. 14. (a) The triple-lens correction system model from LightTools®. The optimal separation (in mm) between the lenses and IRR are indicated for an interrogation distance of 2.5m between the source/detector and the retroreflector. (b) Spot observed on the annular detector ($P_{Detector}$ = 0.975W, P_{Launch} = 1W). The detector has an outer and inner radius of 10mm and 1mm respectively.

The optical correction system designed and optimized for high efficiency operation at a distance of 2.5m is shown in Figure 14a. It is a simple system consisting of three readily available, cheap, off-the-shelf lenses. It redirects the diverging "retroreflected" beam back to the optical axis to achieve true retroreflection. A very high theoretical efficiency of about 97.5% is achieved. Figure 14a also indicates the optical separation between the three lenses and the IRR. For an interrogation distance of 2.5m, the system length is under 7.5cm. The optimized correction system utilized the catalog lenses NT08-016, NT08-034 and NT32-492 (biconvex, biconcave and achromat respectively) from Edmund Optics®. The retroreflected beam evenly illuminates the annular detector as shown in Figure 14b with its centroid

located at (3.81μm, 78.28μm) and a ray distribution position standard deviation of 4.97mm and 5.02mm in the x and y directions respectively. The dependence of optical power incident on the detector with the horizontal and vertical rotation of the module is shown in Figure 15. A FWHM angle of 19.13° and 23.48° in the horizontal and vertical rotational directions respectively is calculated.

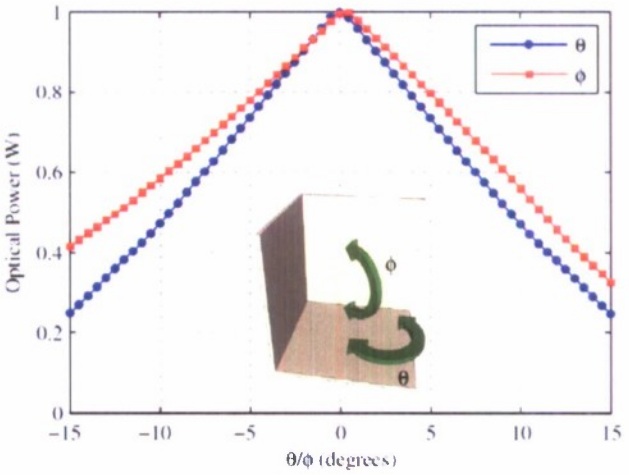

Fig. 15. Theoretical dependence of optical power retroreflected on to the detector by the triple-lens-corrected retroreflector module on the horizontal (θ) and vertical (ϕ) rotation of the module as indicated in the inset. A peak efficiency of about 97.5% is observed.

b. Experimental results

The triple-lens correction system described in the previous sub-section was setup and tested using the experimental setup shown in Figure 16. For the experimental validation of the corrected retroreflection, a circular shaped detector was placed very close to the HeNe laser. A single retroreflected beam is shown illuminating the detector. The dependence of the detector photocurrent is shown in Figure 17. The vertical angle (ϕ) could only be varied from -10° to +4.5° due to the limitation on the angular stage used. The experimental FWHM angle for vertical rotation is approximately 24.43° which matches well with the theoretical prediction. However the experimental FWHM angle for the horizontal (θ) rotation is approximately 15.46°. This slight deviation from the theoretical model is because we used single circular-shaped detector instead of an annular detector. The detector in the experiment is horizontally shifted to

one side of the optical axis while the annular detector extends on both sides of the axis. Hence, the horizontal rotation of the IRR results in a smaller FWHM angle in the experiment.

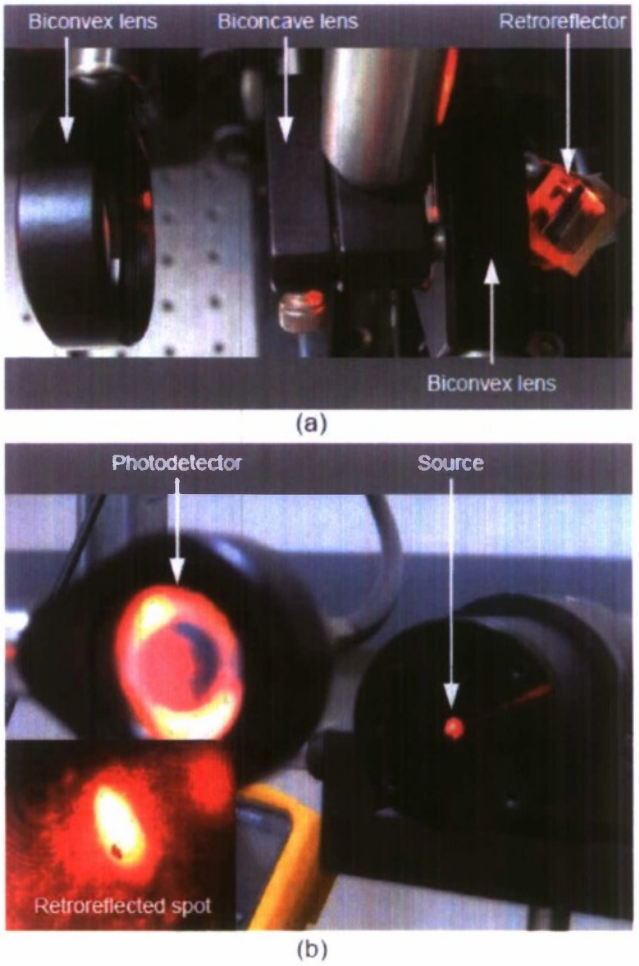

Fig. 16. Experimental setup to test the correction system (top). Also shown is the source-detector setup with the now retroreflected light illuminating the detector (bottom). The bottom-left inset shows the true retroreflected spot.

5. Discussion

The fundamental limit to the switching speed of the device used is the RC time constant. While the system described above can deliver a high CR, the use of large–area MQW devices limits its dynamic performance due to its RC limit. The devices fabricated have a capacitance of about 500pF. This capacitance can be reduced by pixellating the large–area device into individually addressable smaller

devices [1] which keep the total active area high. This pixellation also reduces the probability of a defect in an individual pixel.

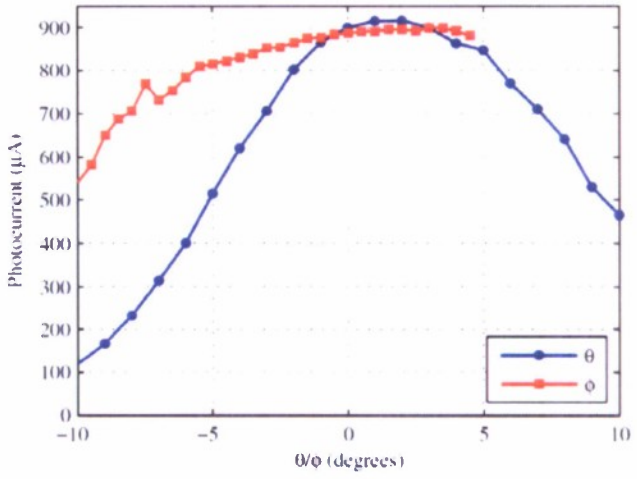

Fig. 17. Experimental result - Dependence of detector photocurrent on the horizontal (θ) and vertical (ϕ) rotation of the IRR.

For an individual device tilted at ~35°, a CR of 4.36dB was measured for a reverse bias of 20V. However, the CR of the combined module was measured to be 8.23dB. There are two possible reasons for this. The AR coating performance is angular dependent. Variation of the illumination angle can have an effect of lowering the CR. Additionally, although the three devices used in the module were from the same substrate, preassembly device testing showed that the excitonic absorption peak occurred at slightly different wavelengths. These result in the broadening of the modules combined excitonic absorption peak. This in turn can result in a lower combined CR.

An important parameter in the free–space optical link enabled by the system described in this paper is the power consumption. The power consumption of the MRR is directly proportional to the square of the driving voltage [1]. Thus, for a given CR, the system proposed here dissipates lesser power.

6. Conclusion

In this work, we demonstrate the use of standard microelectronics packaging technology for the construction of a modulating retroreflector. This MRR consists of three large–area InP–based multiple

quantum well devices operating in the 1550nm region on the three faces of the corner–cube. The quantum well devices fabricated using MOCVD show lower defect density than similar devices fabricated using MBE. The assembled MRR showed a high CR of 8.23dB.

We were unable to meet the targeted manufacturing tolerances (i.e. face angle error of ±0.5°) due to the imprecise PCB manufacturing processes. However, we show that we can correct for the angular error in the 'imperfect' retroreflector using off-the-shelf optical components. The added bulk of an optical correction system may be undesirable for some applications since it introduces pointing accuracy restraints. Hence, we are currently investigating the feasibility of using a precision corner cube to host three PCBs (on which the MQW devices are bonded) on its three faces.

References

[1] G. C. Gilbreath, W. S. Rabinovich, T. J. Meehan, M. J. Vilcheck, R. Mahon, R. Burris, M. Ferraro, I. Sokolsky, J. A. Vasquez, C. S. Bovais, K. Cochrell, K. C. Goins, R. Barbehenn, D. S. Katzer, K. Ikossi-Anastasiou, and M. J. Montes, "Large-aperture multiple quantum well modulating retroreflector for free-space optical data transfer on unmanned aerial vehicles," Optical Engineering, vol. 40(7), pp. 1348–1356, July 2001.

[2] A. Nicholas, G. Gilbreath, S. Thonnard, R. Kessel, R. Lucke, and C. Sillman, "The atmospheric neutral density experiment (ANDE) and modulating retroreflector in space (MODRAS): Combined flight experiments for the space test program," Proceedings of SPIE, vol. 4884, pp. 49–58, June 2003.

[3] T. K. Chan and J. E. Ford, "Retroreflecting optical modulator using an MEMS deformable micromirror array," Journal of Lightwave Technology, vol. 24(1), pp. 516–525, January 2006.

[4] D. H. Parker, M. A. Goldman, B. Radcliff, and J. W. Shelton, "Attenuated retroreflectors for electronic distance measurement," Optical Engineering, vol. 45(7), July 2006.

[5] S. P. Griggs, M. B. Mark, and B. J. Feldman, "Dynamic optical tags," Proc. SPIE, vol. 5441, pp. 151–160, November 2004.

[6] J. Blau, "Car Talk," IEEE Spectrum, p. 16, October 2008.

[7] J. N. Mait, M. W. Haney, K. W. Goossen, and M. P. Christensen, "Shedding light on the battlefield – Tactical applications of photonic technology," Defense & Technology Paper 7, November 2004.

[8] C. Luo and K. W. Goossen, "Optical microelectromechanical system array for free-space retrocommunication," IEEE Photonics Technology Letters, vol. 16, no. 9, pp. 2045–2047, September 2004.

[9] C. Luo and K. W. Goossen, "Free-space optical link by microelectromechanical system array and corner cube retroreflector," IEEE Photonics Technology Letters, vol. 17, no. 6, pp. 1316–1318, June 2005.

[10] D. Pederson and O. Solgaard, "Free space communication link using a grating light modulator," Sens. Act. A, Phys., vol. A83, pp. 6–10, 2000.

[11] C. M. Swenson, C. A. Steed, I. A. DeLaRue, and R. Q. Fugate, "Low power FLC-based retromodulator communications systems," Proc. SPIE, vol. 2290, pp. 296–310, 1997.

[12] B. Perezhki, S. M. Lord, and J. S. Harris, "Electroabsorptive modulators in InGaAs/AlGaAs," Appl. Phys. Lett., vol. 59, pp. 888–890, 1991.

[13] K. W. Goossen, J. E. Cunningham, W. Y. Jan, and R. Leibenguth, "On the operational and manufacturing tolerances of GaAs-AlAs MQW modulators," IEEE J. Quantum Electronics, vol. 34, no. 3, pp. 431–438, March 1998.

[14] K. W. Goossen and D. W. Prather, "Fabrication and yield of large–area quantum–well modulators," IEEE Photonics Technology Letters, vol. 19, no. 24, pp. 2054–2056, December 2007.